Proceedings of the ASME 2018 Symposium on Elevated Temperature Application of Materials for Fossil, Nuclear, and Petrochemical Industries
ETAM2018
April 3-5, 2018, Seattle, WA, USA

ETAM2018-6727

DEVELOPMENT OF CREEP-RESISTANT, ALUMINA-FORMING FERROUS ALLOYS FOR HIGH-TEMPERATURE STRUCTURAL USE

Y. Yamamoto, M.P. Brady, G. Muralidharan, B.A. Pint, P.J. Maziasz, D. Shin, B. Shassere
Oak Ridge National Laboratory
Oak Ridge, TN, USA

S.S. Babu, C.-H. Kuo
University of Tennessee
Knoxville, TN, USA

ABSTRACT

This paper overviews recent advances in developing novel alloy design concepts of creep-resistant, alumina-forming Fe-base alloys, including both ferritic and austenitic steels, for high-temperature structural applications in fossil-fired power generation systems. Protective, external alumina-scales offer improved oxidation resistance compared to chromia-scales in steam-containing environments at elevated temperatures. Alloy design utilizes computational thermodynamic tools with compositional guidelines based on experimental results accumulated in the last decade, along with design and control of the second-phase precipitates to maximize high-temperature strengths. The alloys developed to date, including ferritic (Fe-Cr-Al-Nb-W base) and austenitic (Fe-Cr-Ni-Al-Nb base) alloys, successfully incorporated the balanced properties of steam/water vapor-oxidation and/or ash-corrosion resistance and improved creep strength. Development of cast alumina-forming austenitic (AFA) stainless steel alloys is also in progress with successful improvement of higher temperature capability targeting up to ~1100°C. Current alloy design approach and developmental efforts with guidance of computational tools were found to be beneficial for further development of the new heat resistant steel alloys for various extreme environments.

INTRODUCTION

Over the past several decades, numerous efforts to develop structural alloys with improved high-temperature properties (such as creep strength and/or oxidation resistance) have been made with the goal of providing acceptably long service lives in the extreme environments characteristic of fossil-fueled power generation systems [1,2,3]. Alloy capabilities are sought that would allow operation at increased temperatures and pressures to enable improvements in the efficiency of power generation systems and reduced emissions, and/or their use for manufacturing heat transfer components with decreased wall thicknesses, hence improving their ability to withstand thermal cycling. A major issue to be addressed in the development of alloys for higher temperatures is the property improvements balancing the high-temperature mechanical performances and the environmental compatibilities, since the surface degradation of materials/components during long-time operation could shorten the service life less than that expected only from the material strength. However, the routes for balancing the strengths and the surface protection in a single alloy often are mutually incompatible.

To resolve this dilemma, a new alloy design strategy of "creep-resistant, alumina-forming Fe-base alloys" has been proposed at Oak Ridge National Laboratory (ORNL), initiated from alumina-forming austenitic (AFA) stainless steel alloys, for high-temperature structural applications in fossil-fired power generation systems [4,5,6,7,8,9,10,11]. Protective, external alumina-scale exhibits one to two-orders of magnitude slower oxide growth kinetics compared to chromia-scales, and is far more stable in water vapor containing environments at elevated temperatures [12,13], which significantly reduces potential material failure attributable to surface degradation during service. The key design strategy is to define compositional guidelines to achieve protective alumina-scale formation instead of the chromia-scale formation on conventional stainless steels, and then maximize second-phase precipitate strengthening for high temperatures. Computational thermodynamic tools have been actively utilized for the downselection of the candidate alloy compositions. The alloy

Copyright © 2018 ASME

Downloaded From: http://proceedings.asmedigitalcollection.asme.org/ on 06/18/2018 Terms of Use: http://www.asme.org/about-asme/terms-of-use

design strategy is applicable to not only austenitic stainless steels, but also to ferritic steels such as FeCrAl alloys, with development efforts in progress [14,15].

This paper provides an overview of the recent progress on developing alumina-forming Fe-base alloys for high-temperature structural applications at ORNL. The classes of ferritic and austenitic steel alloys, as well as the recent efforts on developing cast version of AFA alloys, are s ummarized. The contents include the detailed alloy design strategies and property comparison with similar classes of commercially available steel and alloys.

HIGH CR FECRAL FERRITIC ALLOYS

Alloy Design

FeCrAl alloys are historically known to exhibit very high oxidation resistance at elevated temperatures because of the formation of protective, external alumina-scale. Additions of reactive elements such as Y, Hf, Zr, are also known to improve the oxidation resistance through reduced oxide growth rate and enhancing the adhesion between the protective alumina-scale and the ferrite matrix [16,17]. Such excellent oxidation resistance at elevated temperatures, especially in water-vapor containing environments, is also attractive for applications in various extreme environments, such as accident-tolerant fuel cladding in light water reactors [18,19,20]. On the other hand, the high-temperature creep properties of the alloys are poor because of low creep deformation resistance of the ferritic matrix with body-center-cubic (BCC) structure [21]. Unlike ferritic-martensitic steels, FeCrAl alloys consist of a fully ferritic matrix with no phase-transformation to austenite up to the melting point. Because of the low carbon solubility in BCC-Fe matrix, carbides/carbonitrides are not a strong candidate for precipitate strengthening at elevated temperatures. Oxide dispersion strengthened (ODS) FeCrAl alloys overcome the weakness of high-temperature creep property of the alloys [22], although the production cost (e.g. powder processing, consolidation, etc.) is higher than conventional cast-and-wrought processes, and restricts the use of ODS-FeCrAl alloys to niche applications.

The authors recently proposed a new alloy design with a base alloy composition of Fe-30Cr-3Al (wt.%) combined with minor alloy additions of Nb, Zr, Ti, Mo, W, Mn, Si, and C, which yields a "creep-resistant, high Cr containing FeCrAl alloys". The Cr content with ~30 wt.% was selected to improve ash-corrosion resistance in fire-side corrosive environments encountered in fossil-fired power plants [23]. The combined additions of Al and Nb were also found to promote both steam/water vapor oxidation resistance and ash-corrosion resistance [14,15]. The alloys were designed with precipitation strengthening through introduction of Laves phase (C14-Fe_2Nb) precipitate dispersion in BCC-Fe matrix [24]. Similar approaches to strengthen ferritic steels by Laves phase precipitates have also been reported [25,26], which successfully improved creep strength. Computational thermodynamic tools (JMatPro® v.9 with Fe database and Thermo-Calc® with TCFE8) were used to guide the alloy composition range as well as the BCC-solvus temperature to find solution heat treatment temperature ranges. The developmental effort initiated from the "model" alloys consisting of major elements (Fe, Cr, Al, Nb, Si, Ti, Mo, W), and then moved to the "engineering" alloys containing 0.4Mn, 0.15Si, and 0.03C, simulating typical impurities expected in industrial scale production

The high Cr containing FeCrAl alloys were designed to consist of a BCC-Fe single-phase matrix at high temperature (above the solvus temperature, ~900-1200°C) and BCC-Fe + Laves phase at low temperature (below solvus temperature), which allowed fine particle dispersion of Laves phase precipitates through proper heat treatments. The key factors to design the alloys are (1) to increase the amount of second-phase particle dispersions for improved creep resistance, and (2) lower the solvus temperature as possible (below <1200°C, ideally ~1100°C) to allow the solution heat treatment at reasonably low enough temperature to avoid unnecessary grain coarsening and utilize readily achievable industrial heat treatment practices. Figure 1 illustrates the calculated amount of Laves phase at 700°C and the solvus temperatures of the alloys (based on Fe-30Cr-3Al-1Nb-0.4Mn-0.15Si-0.03C) as a function of additional Laves-phase forming elements such as Nb, Ti, Mo, and W. The results demonstrated that both factors increased with increasing the amount of the additional elements. The Ti addition exhibited strongest effect on increasing Laves phase among all elements, and the Nb addition followed. However, the Nb addition also caused an abrupt increase of the solvus temperature. The additions of Mo and W mildly affected to both factors. Note that the amounts of Ti and Mo additions need to be limited due to poisoning effect on the stability of protective alumina-scale [5,7,9] and/or promotion of brittle σ-FeCr or χ-FeCrMo formation [21], respectively. Based on these considerations, a mixed combination of 1Nb-(2 or 6)W-0.3Ti-0.5Mo which maximized the amount of Laves phase at ~700°C range and minimized potential degradation species were selected and proposed for further evaluation as one of the candidate alloying additions in the engineering alloys.

Material Preparation

Lab-scale heats of the model and engineering alloys (~ 500g) were prepared by arc-melting with pure element feedstock, followed by homogenization, hot-forging and -rolling, and then solution heat treatments, to prepare plate-shape samples. The alloy composition ranges are summarized in Table 1. Isothermal tensile creep tests within a range of 650-800°C and 50-150MPa in laboratory air were conducted by using a dog bone shape sheet specimen with the gage size of 0.7 x 3.2 x 13 mm. The creep deformation was measured by using a linear valuable differential transducer attached not to the specimen but the pulling rod, therefore the tests was conducted semi-quantitatively. Cyclic oxidation teat at 800°C

Copyright © 2018 ASME

Downloaded From: http://proceedings.asmedigitalcollection.asme.org/ on 06/18/2018 Terms of Use: http://www.asme.org/about-asme/terms-of-use

in air +10%H2O and ash-corrosion tests were conducted by using 0.8 x10 x 20 mm size coupons and 6 mm diameter x 25 mm length rod specimens, respectively. Details of the ash-corrosion test are summarized in the latter part of this section.

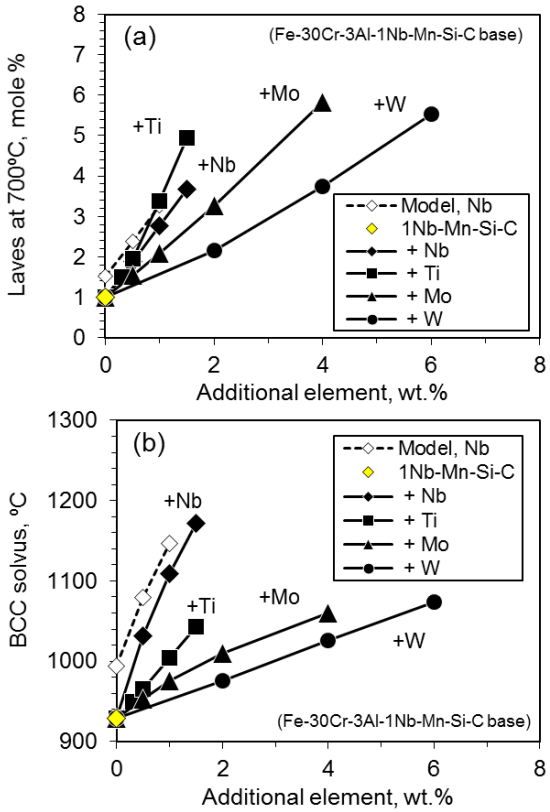

Figure 1. Effects of third element additions on (a) the calculated mole fraction of Laves-phase at 700°C and (b) the BCC solvus temperature in Fe-30Cr-3Al-1Nb-0.4Mn-0.15Si-0.03C base alloys, calculated by JMatPro®.

Table 1. Alloy composition range studied.

	Model alloys	Engineering alloys
Base alloy, wt.%	Fe-30Cr-3Al-0.2Si	Fe-30Cr-3Al-1Nb-0.4Mn-0.15Si-0.03C-0.05Y
Alloying additions, wt.%	(0, 1, or 2)Nb, 1Nb-(0.1 or 0.3)Zr, 1Nb-(0.5 or 1)Ti, 1Nb-2W	0.5Mo-0.3Ti-2W, 0.5Mo-0.3Ti-6W
Remarks	Also prepared 25Cr-3Al-2Nb alloy & 30Cr-2.6Al-2Nb alloy	Simulating industrial grade

Creep Performance

Figure 2 illustrates the relationship between experimentally obtained minimum creep rates of the model/engineering alloys tested at 700°C and 70MPa, and the amounts of the calculated Laves phase at 700°C. The larger amount of Laves phase, the higher resistance of creep deformation achieved at the given test condition. The engineering alloys showed a little less creep resistance than the model alloys, which could be due to the formation of other second-phase particles (e.g. carbides) affecting the kinetics of strengthening Laves phase precipitates negatively. The obtained minimum creep rates were also affected by other microstructural factors such as grain size, precipitate size, and precipitation kinetics, although microstructure observation indicated that the variations of these factors among the alloys were small enough to be negligible in the current discussion. This suggests that further improvement of creep properties is expected by controlling and optimizing such microstructural factors.

Figure 3 shows the Larson Miller Parameter plot, LMP {= (T [°C]+273) x (C + log $t_{rupture}$[h]), where T is test temperature, $t_{rupture}$ is creep-rupture life, and C is a constant (C=20)} of the model alloy (2Nb, tested in a range of 650-750°C) and the engineering alloy (1Nb-6W, 700-800°C). The LMPs of commercial ferritic-martensitic (F-M) steels (Gr. 91 and Gr. 92, 9Cr-1Mo and 9Cr-2W base, respectively) and austenitic stainless steel (TP347HFG, 18Cr-11Ni-Nb-C base) [27] are also shown for comparison. The model alloy showed similar creep strength to Gr. 92, and the engineering alloy exhibited nearly 50% larger creep strength than Gr. 92 which was close to that of TP347HFG. These results suggest that Laves phase precipitate strengthening is effective to improve the high-temperature creep performance of Fe-30Cr-3Al base alloys.

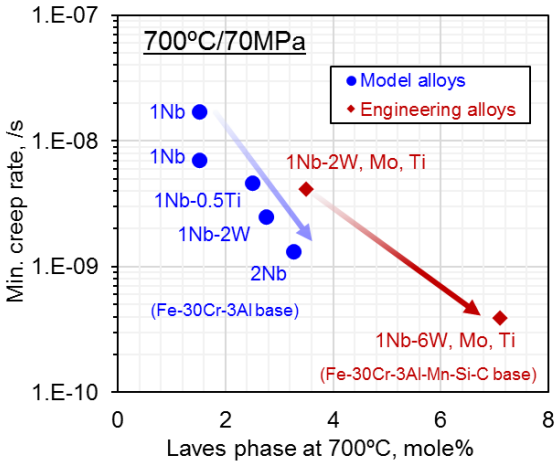

Figure 2. Minimum creep rates of Fe-30Cr-3Al base "model" and "engineering" alloys with third element additions at 700°C and 70MPa, plotted as a function of the calculated amount of Laves phase at 700°C.

Water Vapor Oxidation Resistance

Oxidation test results at 800°C in air with 10% water vapor suggest that the combination of high Cr, Al, and Nb is the key to obtain better oxidation resistance, as shown in Figure 4. The binary Fe-25Cr and Fe-30Cr alloys (reference materials) showed a rapid weight gains, followed by significant weight loss after only 300h testing. This was due to the formation of chromia-scales in the early stage of oxidation, and then further reaction of chromia and water-vapor resulting in the formation

Copyright © 2018 ASME

Downloaded From: http://proceedings.asmedigitalcollection.asme.org/ on 06/18/2018 Terms of Use: http://www.asme.org/about-asme/terms-of-use

of volatile $CrO_2(OH)_2$ [28]. On the other hand, all FeCrAl alloys showed very slow oxidation kinetics for up to ~5,000h (longer duration exposures are currently in progress). The initial mass gain was insensitive to the Al content when compared the alloys with 3Al and 2.6Al. The mass gains of the alloys with low Cr (25 wt.%) and the Ti containing alloys were relatively higher than the others, but still showed very slow oxidation kinetics. The engineering alloy with 1Nb-6W exhibited a little faster mass gain compared to the model alloys, although the amount was still low compared to the reference materials.

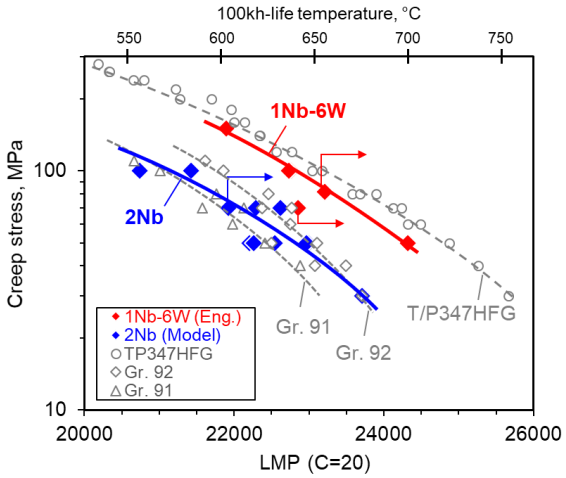

Figure 3. Larson-Miller Parameter plot of model (2Nb) and engineering (1Nb-6W) alloys comparing with commercial ferritic-martensitic steels (Gr. 91 and Gr. 92) and austenitic stainless steel (TP347HFG) [27]. The allows indicate that the tests are in progress.

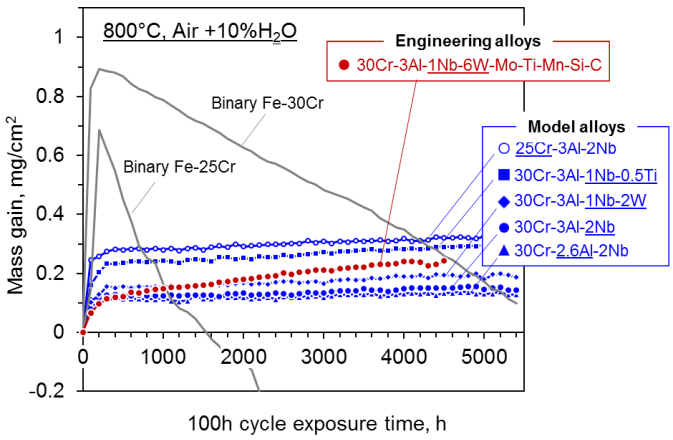

Figure 4. Mass gain of high-Cr containing FeCrAl alloys and binary Fe-Cr alloys after cyclic exposure testing at 800°C in air + 10% water vapor.

Ash-corrosion Resistance

Ash-corrosion test was performed by immersing the rod-shape specimens of the model/engineering alloys into a synthetic ash consisting of various oxides, hydroxides and sulfates, together with a flowing mixed gas, which simulated a combustion environment in fossil-fired power plants. The detailed components are summarized in Table 2 [15]. The test was conducted at 700°C for 500h. The specimens after testing, together with mass change of the specimens, are shown in Figure 5. Note that the mass change does not always reflect the degree of surface damage from corrosion, but it still can be used as one of the degradation metrics if it was combined with the characterization of surface conditions. The model alloys with 2Nb (Figs. 5a through 5c) indicated that the corrosion resistance was insensitive to Al contents in the range of 2.6 to 3 wt.%, whereas the surface protection was significantly lost by decreasing the Cr content from 30 to 25 wt.%. The mass change also indicated a significant material loss in the low Cr containing alloy. On the other hand, reduction of Nb to 1 wt.% combined with W additions (5d and 5e) would not significantly impact the corrosion resistance of the alloys.

Table 2. Components of synthetic ash and gas [15].

Media	Components
Ash	Al_2O_3, SiO_2, CaO, Fe_2O_3, KOH, TiO_2, MgO, $Fe_2(SO_4)_3$, $MgSO_4$, K_2SO_4, Na_2SO_4
Gas	N_2, CO_2, H_2O, O_2, SO_2

Considering all results, the engineering alloy with 1Nb-6W-0.3Ti-0.5Mo possesses the most balanced mechanical properties and environmental compatibilities for high-temperature structural material applications. A scale-up effort of the alloy has been initiated by preparing ~ 30 kg ingot through a commercial vacuum induction melting process for further evaluate the properties of the alloy including processability, long-term creep property, toughness, and weldment. The comprehensive property evaluation of high Cr containing FeCrAl alloy will be summarized and reported elsewhere.

Copyright © 2018 ASME

Downloaded From: http://proceedings.asmedigitalcollection.asme.org/ on 06/18/2018 Terms of Use: http://www.asme.org/about-asme/terms-of-use

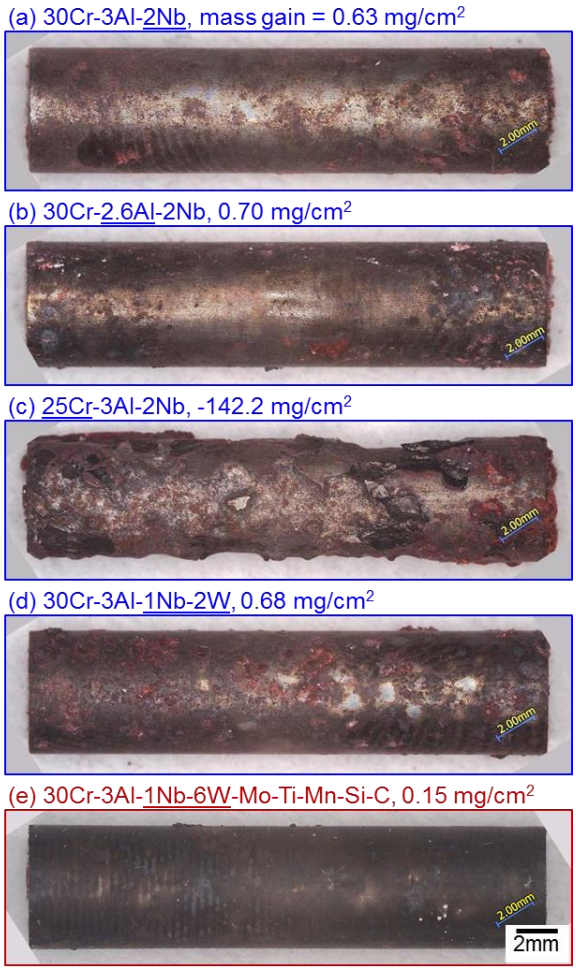

Figure 5. Rod specimens of high-Cr containing FeCrAl alloys exposed in a synthetic gas and mixed ashes (at 700°C for 500h) simulating a combustion environment in fossil-fired power plants.

ALUMINA-FORMING AUSTENITIC (AFA) ALLOYS

Alloy Design

Early development efforts of AFA stainless steels originated in the 1970's [29,30,31,32,33,34]. The additions of Al (and Cr) need to be limited at given Ni contents for maintaining a single-phase austenite matrix for creep strength, which always need to be compromised with the formation ability of the protective alumina. Recently, a new family of AFA stainless steels with a promising combination of mechanical properties and oxidation resistance has been developed at ORNL [4-11]. The balanced properties of the creep and oxidation resistance have been realized in a broad base composition range of Fe-(12-35)Ni-(12-19)Cr-(2.5-4)Al-(0.6-3)Nb (in wt.%) with balanced levels of alloying additions, primarily Al, Cr, Mn, and Ni, to maintain a single phase austenitic matrix microstructure and alumina-scale formability with guide from computational thermodynamic tools. Combination with strengthening second-phases such as MC (M: primarily Nb), $M_{23}C_6$ (M: primarily Cr) [5,34,35], or γ′-Ni_3Al precipitates successfully achieved the improved creep strength [6,10,11]. Alloying additions recently investigated including B, C, Cu, Mn, Mo, Si, etc. to further balance mechanical properties and oxidation resistance [6,9,36,37,38,39]. Figure 6 summarizes the effect of alloying additions on various AFA alloy properties which were accumulated during the developmental efforts at ORNL.

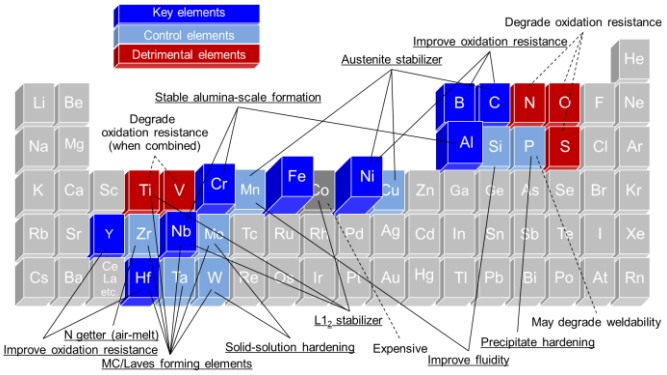

Figure 6. A periodic table summarizing elemental effects on AFA alloy properties.

Classification of AFA Grades

The developed AFA alloys to date can be classified into three different grades, based on the Ni contents and the target temperatures for alumina-scale formation, as summarized in Table 3. The "standard" AFA grade contains 20-25 wt.% Ni which targets the temperature range from 750-950°C. The major strengthening precipitates are MC and/or $M_{23}C_6$. The low nickel containing AFA grade, so-called "AFA^{LN}", requires relatively low Ni content by additions of Mn and Cu to support the stability of austenite matrix. The Al addition is also limited which results the target temperature range lower than the standard grade. The high nickel containing AFA with $L1_2$ strengthening utilizes coherent γ'-Ni_3Al formation for high-temperature strengthening, which offers the use with the requirement of relatively high strength.

Table 3. Three different wrought AFA grades

Grade	Composition, wt.%	Target
AFA Grade	Fe-(14-15)Cr-(2.5-4)Al-(20-25)Ni-(1-3)Nb with Mn, Si, C, B, Mo, W, Hf, Y, etc.	~750-950°C for Al_2O_3 formation, MC and $M_{23}C_6$ strengthening
Low Nickel AFA^{LN}	Fe-14Cr-2.5Al-(12-15)Ni-0.6Nb-(5-10)Mn-3Cu with Si, C, B, etc.	~650-700°C for Al_2O_3 formation, $M_{23}C_6$ and Cu strengthening
High Nickel AFA with $L1_2$ strengthening	Fe-(14-19)Cr-(2.5-3.5)Al-(30-35)Ni-3Nb with Ti, Si, C, B, etc.	~750-850°C for Al_2O_3 formation, γ'-Ni_3Al strengthening

Copyright © 2018 ASME

Downloaded From: http://proceedings.asmedigitalcollection.asme.org/ on 06/18/2018 Terms of Use: http://www.asme.org/about-asme/terms-of-use

Representative creep-rupture properties of three different AFA grades are summarized in Figure 7. Two standard AFA grade alloys exhibited different range of creep strengths; the alloy with 20Ni-1Nb-0.2C was optimized for creep strength through maximizing MC/$M_{23}C_6$ strengthening effects, whereas the alloy with 25Ni-2.5Nb-0.1C leaned toward better oxidation resistance with high Ni and Nb contents which compromised its creep strength. Both were in the range of creep strengths between standard 347 austenitic stainless steel (18Cr-11Ni-Nb-C base) and Alloy 709 (20Cr-25Ni-Mo-Nb-C-N). The creep strength of AFA^{LN} grade alloy followed the standard AFA grade with 20Ni-1Nb-0.1C. The raw material cost of AFA^{LN} would be comparable to standard 347 steel [40], so that the AFA^{LN} alloy potentially possesses high cost-effectiveness. AFA alloy with $L1_2$ strengthening achieved the creep strength comparable to Ni base alloy 617. However, the creep strength became low at 750°C since the fraction of $L1_2$ phase significantly dropped in the temperature range. For higher temperature capability, the modification of the alloy composition is currently in progress.

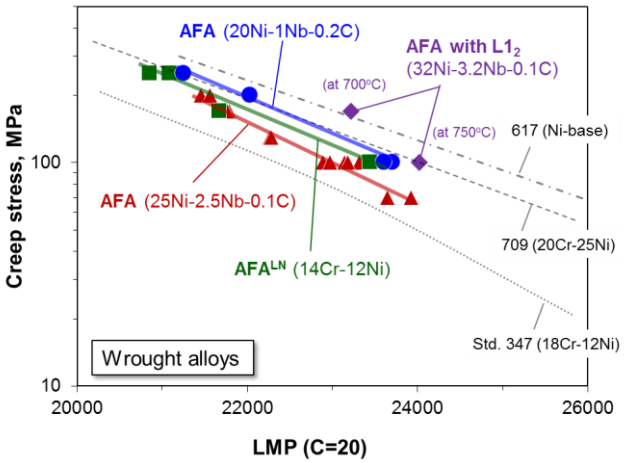

Figure 7. LMP plot of three different AFA grades (including two different standard AFA grade alloys), together with those of commercially available austenitic stainless steels (347: 18Cr-11Ni, 709: 20Cr-25Ni base) and Ni-base alloy 617 [4-11,40].

Environmental Compatibilities

Improved oxidation resistance of the developed AFA alloys in air and air + water vapor has been evaluated and discussed in numerous reports [5,7,8,9,40]. However, recent industrial demands are interested in potential protective effects of alumina-scale in various extreme environments, such as coking, metal dusting, supercritical CO_2, molten salt, liquid metal, etc. Evaluation of a mixed environment compatibility (oxidation and sulfidation) was recently reported, as shown in Figure 8 [40], which represented a limited metal loss of AFA alloys during exposure in a sulfidation-oxidation condition at 550 and 650°C. By comparing with commercial austenitic stainless steels 310 (25Cr-20Ni base) and 347 (18Cr-11Ni base), the AFA alloys showed similar or even better protectiveness in such aggressive environments, especially at higher temperatures. Although further comprehensive evaluation is still required, it is suggested that the AFA alloys offer potential environmental compatibilities in not only steam/water vapor oxidation environments but also the mixed corrosive environments as well.

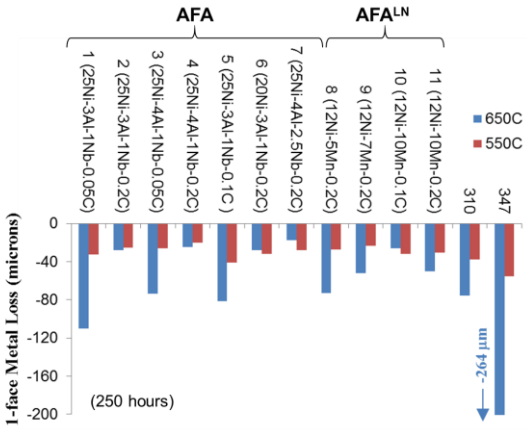

Figure 8. Metal loss assessed by sectioning from samples exposed for 250 h at 550 and 650°C sulfidation-oxidation conditions of Ar-20% H_2-5% H_2S-20% H_2O (after reference [40])

Potential Applications

One of the potential applications for AFA alloys is a heat-exchanger since thin-foil components have a large surface area/volume ratio in which the surface protection is a critical requirement for the component life. Field trials of an AFA alloy foil material in a turbine-based combined heat and power (CHP) systems have been performed by using commercially rolled AFA foil with widths over 39 cm [41]. The heat exchanger was fabricated as recuperator air cell components by using the folded AFA alloy foil, as shown in Figure 9. The first trial completed 3,000 h in a microturbine recuperator with an elevated turbine inlet temperature, which exhibited limited degradation. A longer microturbine trial with more than 16,000h is also in progress.

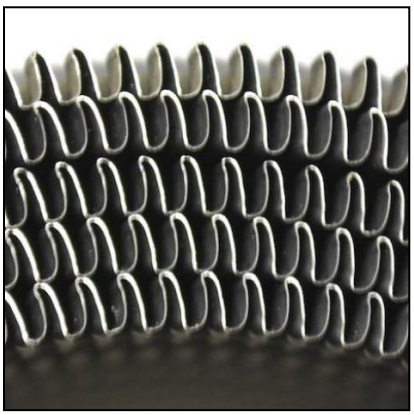

Figure 9. Folded AFA alloy foil for use in a turbine recuperator air cell component trial (after reference [42])

Copyright © 2018 ASME

Downloaded From: http://proceedings.asmedigitalcollection.asme.org/ on 06/18/2018 Terms of Use: http://www.asme.org/about-asme/terms-of-use

Alloy Design through Materials Informatics Approach

One of the approaches to minimize the development time is to utilize computational pathway with proper (and sufficiently large numbers of) experimental dataset within the context of data analytics. Because of numbers of the wrought AFA developmental efforts in the last decade, there are more than 100 of different alloy compositions and creep-rupture test data accumulated at ORNL. The authors are using materials informatics approach, i.e. correlation analysis and machine learning techniques, to predict LMP of AFA alloys as a function of composition and creep stress. Surrogate machine learning models with ORNL creep dataset (see Figure 10) successfully output the predicted LMPs with an accuracy around 90%. This data analytics-based approach allows predicting LMP of hypothetical AFA alloys, but it should be only used to qualitatively compare the creep properties of different alloys. In addition, the current approach only takes elemental composition as input features cannot generate any alloy hypothesis that can be used to better understand underlying mechanisms. Approaches to incorporate other factors are in progress.

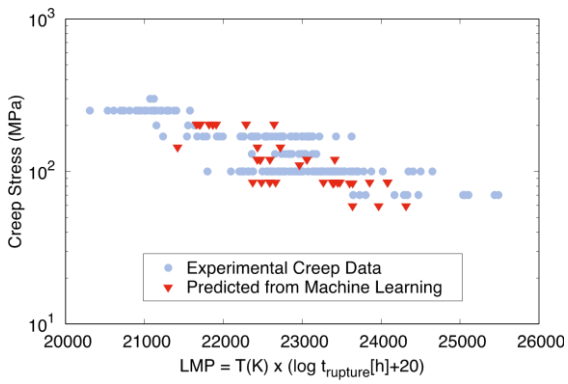

Figure 10. LMP plot showing creep-rupture test results of all wrought AFA alloys to date, together with predicted LMP by using a machine learning approach at ORNL to date (preliminary analysis data).

CAST AFA ALLOYS

Alloy Design of Cast AFA Alloys

Cast austenitic stainless steels are widely used in various high-temperature structural applications such as furnace rollers, heat exchangers, exhaust manifolds and turbocharger housing in personal/commercial vehicles, chemical/petrochemical process tubes, at temperatures up to 1150°C [43]. The class of cast austenitic alloys of interest in the current study included HK (25Cr-20Ni-0.4C) and HP (25Cr-35Ni-0.4C) which relies on chromia-scale formation for the surface protection and MC (M: mainly Nb) and $M_{23}C_6$ (M: mainly Cr) dispersions in austenite matrix for high temperature strength [44,45,46,47,48]. Since many industrial environments contain water vapor, AFA could offer a strong advantage in surface protection, and therefore the component life, compared to commercially available cast austenitic stainless steels. Alloy design should also incorporate the controlled microstructure to introduce sufficient high-temperature strength.

In cast AFA alloy development, non-equilibrium matrix in as-cast (as solidified) condition was utilized for optimization of strengthening carbide dispersion. The efforts initiated by preparing and evaluating a cast version of wrought AFA alloy with the composition of Fe-14Cr-2Mn-25Ni-3.5Al-2.5Nb-0.1C, wt.%. Two modified alloys containing 1Nb-0.2C and 1Nb-0.5C were also prepared. The analyzed contents of Nb and C, as well as the creep-rupture life of the alloys at 750°C and 100MPa, are summarized in Table 4. The modification improved the creep properties significantly with >20 times longer creep life than the base alloy, and ~50% better creep strength than HK series (based on LMP comparison) [49].

Table 4. Nb and C contents of cast AFA alloys (Fe-14Cr-2Mn-25Ni-3.5Al base with minor additions of Cu, Mo, W, B, and P), together with the creep-rupture life at 750°C and 100MPa [49].

Alloy	Composition, wt.%		Creep-life at 750C/100MPa, h
	Nb	C	
Base (2.5Nb-0.1C)	2.49	0.09	497
#1 (1Nb-0.2C)	0.95	0.20	2299
#5 (1Nb-0.5C)	0.88	0.45	10326

Computational thermodynamic tools suggested that major source of the improved creep properties was the formation of $M_{23}C_6$. Table 5 summarizes the predicted second phases in as-solidified condition (by Scheil calculations) and in equilibrium condition at 750°C. B2-NiAl and Fe_2Nb-Laves phases exhibited large amount of supersaturation, although these precipitates would not dominantly improve/degrade the creep performance [6]. MC would be preferred for precipitate strengthening, although the cast AFA alloy cannot rely on it since the solidification state already exhibited some amounts of MC close to or even more than the equilibrated amount at 750°C. M_6C and M_7C_3 also showed a similar trend. On the other hand, the amount of $M_{23}C_6$ increased significantly at 750°C, and the higher carbon additions resulted in greater amounts of $M_{23}C_6$. A transmission electron microscope (TEM) bright field image of the creep-ruptured Alloy #5, shown in Figure 11, clearly indicated the pinning of dislocations by fine $M_{23}C_6$ carbides with ~100 nm size which effectively increased the creep deformation resistance.

It should be emphasized that the oxidation resistance of the cast AFA alloys at 800°C in air + 10% water vapor were also evaluated. These alloys exhibited slow oxidation kinetics similar to the wrought AFA alloys discussed above [4], and the increased carbon content (up to ~0.3 wt.%) was found to be beneficial for oxidation resistance as well. In order to balance

Copyright © 2018 ASME

Downloaded From: http://proceedings.asmedigitalcollection.asme.org/ on 06/18/2018 Terms of Use: http://www.asme.org/about-asme/terms-of-use

with the creep performance, the carbon range from 0.3~0.5 wt.% was found to attractive for further development of cast AFA alloys.

Table 5. Predicted wt.% of phases present after solidification (Scheil calculations) and equilibrium wt.% (Eq.) of phases in various cast AFA alloys at 750°C [49]

Alloys		Predicted fraction of phases, wt.%					
		B2-NiAl	Fe_2Nb-Laves	MC	$M_{23}C_6$	M_6C	M_7C_3
Base	Scheil	1.5	2.5	0.7	-	-	-
	Eq.	9.2	5.0	0.9	-	-	-
#1	Scheil	0.3	-	0.9	-	0.8	-
	Eq.	9.9	2.9	0.7	2.8	-	-
#5	Scheil	-	-	1.0	0.6	1.2	1.4
	Eq.	9.5	2.1	0.8	7.0	-	-

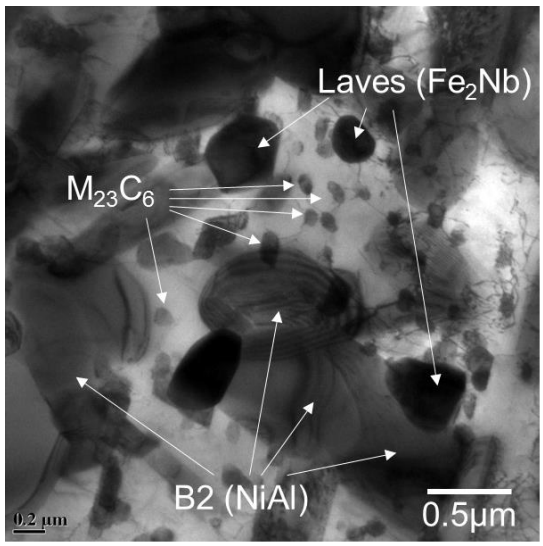

Figure 11. TEM bright field image of Alloy #5 after creep-rupture testing at 750°C, 100MPa.

Further Development and Potential Applications

Modification of cast AFA alloys for higher temperature capability, targeting the service temperatures up to ~1100°C, was initiated at Oak Ridge National Laboratory with a support from commercial manufacturers. One of potential applications is a furnace roller which requires centrifugal casting to make a thick wall tubes. The trial fabrication of centrifugally cast AFA alloy tubes was successfully performed, as shown in Figure 12, without any defect formation attributing the industrial cast process pathway. The design strategy to maximize $M_{23}C_6$ formation described above, in conjunction with further alloying additions/controls to optimize fluidity of liquid metals, solid-solution hardening, another second-phase precipitate strengthening, oxidation resistance, and weldability, has been applied. The best cast AFA alloy to date achieved better creep performance than HP alloys at 1150°C, and excellent oxidation resistance at 1100°C with air + 10% water vapor [50].

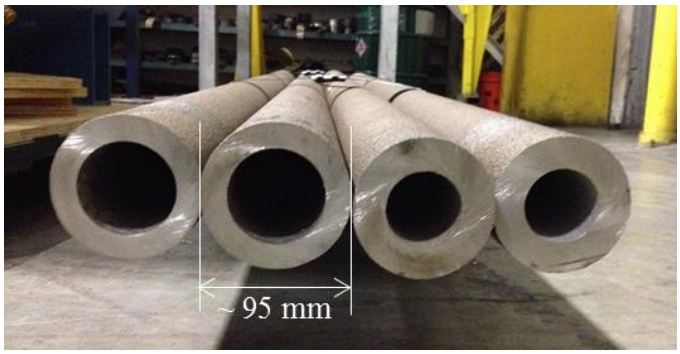

Figure 12. Centrifugally cast AFA alloy tubes

SUMMARY

The recent progresses of alumina-forming Fe-base alloy development at ORNL have been summarized. For the class of ferritic steels, creep-resistant, high Cr containing FeCrAl alloys were proposed with the base alloy composition of Fe-30Cr-3Al-1Nb-6W-Ti-Mo-Mn-Si-C (in wt.%). The alloy successfully achieved creep strengths superior to Gr. 92 F-M steel and comparable to TP347HFG, together with high surface protectiveness in water-vapor containing environments at 800°C and inside an ash-corrosion circumstance at 700°C simulating combustion environments in fossil-fired power plants. Development of alumina-forming austenitic (AFA) stainless steel alloys is in progress by utilizing computational thermodynamic tools with compositional guidelines based on experimental results accumulated in the last decade. Environmental compatibility in various extreme environments is also being evaluated to utilize the potential advantage of protectiveness of external alumina-scale. Alloy design through materials informatics approach has also been initiated through surrogate machine learning models combined with experimentally obtained dataset of AFA alloys at ORNL. Cast AFA alloy development activities achieved better creep performance than HP alloys at 1150°C, and excellent oxidation resistance at 1100°C with air + 10% water vapor. Further compositional optimization is currently in progress for targeting commercialization of the alloys/products.

ACKNOWLEDGMENTS

The authors thank Drs. Dean Pearce and Zhiqian Sun for their reviews and comments on this manuscript, and Dr. Edgar Lara-Carzio for his thoughtful supports on the project. Research sponsored by the Fossil Energy Crosscutting Research Program, Office of Fossil Energy, U.S. Department of Energy (US-DOE), and through a user project supported by ORNL's Center for Nanophase Materials Sciences (CNMS),

Copyright © 2018 ASME

Downloaded From: http://proceedings.asmedigitalcollection.asme.org/ on 06/18/2018 Terms of Use: http://www.asme.org/about-asme/terms-of-use

which is sponsored by the Scientific User Facilities Division, Office of Basic Energy Sciences, U.S. Department of Energy. A part of the research is also funded by the Advance Manufacturing Office (AMO, formerly Industrial Technologies Program, ITP) under Office of Energy Efficiency and Renewable Energy (EERE), US-DOE, the Technology Innovation Program (TIP) under Laboratory Directed Research and Development Program (LDRD) at ORNL, the Seed Money Funds under LDRD at ORNL, and Advanced Research Projects Agency-Energy (ARPA-E) under US-DOE.

This manuscript has been authored by UT-Battelle, LLC under Contract No. DE-AC05-00OR22725 with the U.S. Department of Energy. The United States Government retains and the publisher, by accepting the article for publication, acknowledges that the United States Government retains a non-exclusive, paid-up, irrevocable, world-wide license to publish or reproduce the published form of this manuscript, or allow It others to do so, for United States Government purposes. The Department of Energy will provide public access to these results of federally sponsored research in accordance with the DOE Public Access Plan (http://energy.gov/downloads/doe-public-access-plan).

REFERENCES

[1] R. Viswanathan and W. Bakker: J. Mater. Eng. Perf., 2001, vol. 10, pp. 81–95.
[2] R. Viswanathan and W. Bakker: J. Mater. Eng. Perf., 2001, vol. 10, pp. 96–101.
[3] R. Viswanathan, R. Purgert, and P. Rawls: Adv. Mater. Processes, 2008, Aug., pp. 41-45.
[4] M.P. Brady, Y. Yamamoto, M.L. Santella, P.J. Maziasz, B.A. Pint, and C.T. Liu: JOM, 2008, vol. 60 (7), pp. 12–18.
[5] Y. Yamamoto, M.P. Brady, Z.P. Lu, P.J. Maziasz, C. Liu, B.A. Pint, K.L. More, H.M. Meyer, and E.A. Payzant: Science, 2007, vol. 316 (5823), pp. 433–36.
[6] Y. Yamamoto, M. Brady, M. Santella, H. Bei, P. Maziasz, B. Pint, Metall. Mater. Trans. A-Phys. Metall. Mater. Sci. 42A (2011) 922–931.
[7] M.P. Brady, Y. Yamamoto, M.L. Santella, and B.A. Pint: Scripta Mater., 2007, vol. 57 (12), pp. 1117–20.
[8] M.P. Brady, Y. Yamamoto, B.A. Pint, M.L. Santella, P.J. Maziasz, and L.R. Walker: Mater. Sci. Forum, 2008, vols. 595–598, pp. 725–32.
[9] M.P. Brady, Y. Yamamoto, M.L. Santella, and L.R. Walker: Oxid. Met., 2009, vol. 72 (5–6), pp. 311–33.
[10] Y. Yamamoto, M. Takeyama, Z.P. Lu, C.T. Liu, N.D. Evans, P.J. Maziasz, M.P. Brady, Intermetallics 16 (2008) 453–462.15.
[11] Y. Yamamoto, G. Muralidharan, M.P. Brady, Scr. Mater. 69 (2013) 816–819.
[12] E.J. Opila, Mater. Sci. Forum 461–464, 765 (2004).
[13] E.J. Opila, N.S. Jacobson, D.L. Myers, and E.H. Copland, JOM 58, 22 (2006).
[14] Y. Yamamoto, S.S. Babu, B. Shassere, X. Yu, Proceedings of 123HiMAT-2015 (2015, Sapporo, Japan), the 123rd Committee on Heat Resisting Materials and Alloys, Japan Society for the Promotion of Science, pp.66-69 (2015).
[15 Y. Yamamoto, B.A. Pint, B. Shassere, S.S. Babu, Advances in Materials Technology for Fossil Power Plants_Proceedings from the eighth international conference, Pages 319 – 326 (Oct 2016)
[16] B.A. Pint, J. American Ceramic Society, 86 (2003) 686-695.
[17] B.A. Pint, Oxidation of Metals, 45 (1995) 1-37.
[18] K.A. Terrani, S.J. Zinkle, L.L. Snead, J. Nucl. Mater 448 (2014) 420-435.
[19] Y. Yamamoto, B.A. Pint, K.A. Terrani, K.G. Field, Y. Yang, L.L. Snead, J. Nucl. Mater 467 (2015) 703-716.
[20] Z. Sun, P.D. Edmondson, Y. Yamamoto, Acta Mater. 144 (2018) 716-727.
[21] L. Colombier and J. Hochmann: Stainless and Heat Resisting Steels, St. Martin's Press, New York, NY, 1968.
[22] F.G. Wilson, B.R. Knott, and C.D. Desforges, Met. Mater. Trans. A, 9 (2) (1978), pp. 275–282.
[23] B.A. Pint, J.K.Thomson, Materials and Corrosion, 65, 2 (2014) pp. 132-140.
[24] B. Shassere, Y. Yamamoto, S.S. Babu, J. Poplawsky, W. Guo, Met. Mater. Trans. A, 48 (2017) 4598 – 4614.
[25] Toda, Y., Auchi, M., Sawada, M. K., Kushima, H., Kimura, K., Proceedings of the 10th Liège Conference: Materials for Advanced Power Engineering 2014, B. Kuhn et al (Eds.), September 2014; pp. 239-247.
[26] Kuhn B., and Talik, M., Proceedings of the 10th Liège Conference: Materials for Advanced Power Engineering 2014, B. Kuhn et al (Eds.), September 2014; pp. 264-273.
[27] National Institute of Materials and Sciences (NIMS) creep data sheet, http://smds.nims.go.jp/creep/index_en.html
[28] P.J. Meschter, E.J. Opila, N.S. Jacobson, Annual Review of Materials Research, 43 (2013) 559-588.
[29] T. Fujioka, M. Kinugasa, S. Iizumi, S. Teshima, I. Shimizu, US Patent 3,989,514, Nov 2, 1976.
[30] J.A. McGurty, US Patent 4,086,085, April 25, 1978.
[31 J.C. Pivin, D. Delaunay, C. Roquescarmes, A.M. Huntz, P. Lacombe, Corrosion Sci.20 (1980) 351–373.
[32] B.A. Pint, R. Peraldi, P.J. Maziasz, Proceedings of High Temperature Corrosion and Protection of Materials 6, Part 1 and 2, Trans Tech, 461–464 (2004) 815-822.
[33] V. Ramakrishnan, J.A. McGurty, N. Jayaraman, Oxid. Metals 30 (1988) 185–200.
[34] D.V.V. Satyanarayana, G. Malakondaiah, D.S. Sarma, Mater. Sci. Eng. A-Struct. Mater. Prop. Microstruct. Process. 323 (2002) 119–128.
[35] F.H. Stott, G.C. Wood, J. Stringer, Oxid. Metals 44 (1995) 113–145.
[36] X.Q. Xu, X.F. Zhang, G.L. Chen, Z.P. Lu, Mater. Lett. 65 (2011) 3285–3288.

Copyright © 2018 ASME

Downloaded From: http://proceedings.asmedigitalcollection.asme.org/ on 06/18/2018 Terms of Use: http://www.asme.org/about-asme/terms-of-use

[37] X.Q. Xu, X.F. Zhang, X.Y. Sun, Z.P. Lu, Oxid. Metals 78 (2012) 349–362.
[38] X.Q. Xu, X.F. Zhang, X.Y. Sun, Z.P. Lu, Corrosion Sci. 65 (2012) 317–321.
[39] M.P. Brady, K. Unocic, M. Lance, M. Santella, Y. Yamamoto, L. Walker, Oxid. Metals 75 (2011) 337–357.
[40] M.P. Brady, J. Magee, Y. Yamamoto, D. Helmick, L.Wang, Mater. Sci. Eng. A, 590 (2014) 101-115.
[41] B.A. Pint, S. Dryepondt, M.P. Brady, Y. Yamamoto, B. Ruan, R.D. McKeirnan, Jr., 2015, ASME Paper #GT 2015-42763, presented at the International Gas Turbine & Aeroengine Congress & Exhibition, Montreal, Canada, June 15-19, 2015.
[42] B.A. Pint, S. Dryepondt, M.P. Brady, Y. Yamamoto, 2013, ASME Paper #GT2013-94940, presented at the International Gas Turbine & Aeroengine Congress & Exhibition, San Antonio, TX, June, 3-7, 2013.
[43] Steel Castings Handbook, Supplement 9, High Alloy Data Sheets: Heat Series (Crystal Lake, IL: Steel Founders' Society of America, 2004), pp. 2–60.
[44] H. Wen-Tai and R.W.K. Honeycombe, Mater. Sci. Technol. Ser. 1, 385 (1985).
[45] G.D. Barbabela, L.H. de Almeida, T.L. da Silveira, and I. Le May, Mater. Charact. 26, 1 (1991).
[46] C.W. Thomas, M. Borshevsky, and A.N. Marshall, Mater. Sci. Technol. Ser. 8, 390 (1992).
[47] R.A.P. Ibanez, G.D. de Almeida Soares, L.H. de Almeida, and I. Le May, Mater. Charact. 30, 243 (1993).
[48] I.A. Sustaita-Torres, S. Haro-Rodriguez, M.P. Guerrero-Mata, M. de La Garza, E. Valdes, F. Deshcaux-Beaume, and R. Colas, Mater. Chem. Phys. 133, 1018 (2012).
[49] G. Muralidharan, Y. Yamamoto, M.P. Brady, L.R. Walker, H.M. Meyer III, D.N. Leonard, JOM, 68 (2016) 2803-2810.
[50] M.P. Brady, G. Muralidharan, Y. Yamamoto, B.A. Pint, Oxidation of Metals, 87 (2017) 1-10.

Copyright © 2018 ASME

Downloaded From: http://proceedings.asmedigitalcollection.asme.org/ on 06/18/2018 Terms of Use: http://www.asme.org/about-asme/terms-of-use